The Company of Biologists

RESEARCH ARTICLE

Temporally regulated cell migration is sensitive to variation in body size

Clément Dubois[1,*], Shivam Gupta[2,*], Andrew Mugler[2,3,‡] and Marie-Anne Félix[1,‡]

ABSTRACT

Few studies have measured the robustness to perturbations of the final position of a long-range migrating cell. In the nematode *Caenorhabditis elegans*, the QR neuroblast migrates anteriorly, while undergoing three division rounds. We study the final position of two of its great-granddaughters, the end of migration of which was previously shown to depend on a timing mechanism. We find that the variance in their final position is similar to that of other long-range migrating neurons. As expected from the timing mechanism, the position of QR descendants depends on body size, which we varied by changing maternal age or using body size mutants. Using a mathematical model, we show that body size variation is partially compensated for. Applying environmental perturbations, we find that the variance in final position increased following starvation at hatching. The mean position is displaced upon a temperature shift. Finally, highly significant variation was found among *C. elegans* wild isolates. Overall, this study reveals that the final position of these neurons is quite robust to stochastic variation, shows some sensitivity to body size and to external perturbations, and varies in the species.

This article has an associated 'The people behind the papers' interview.

KEY WORDS: Cell migration, Neuroblast, Robustness, Body size, *C. elegans*

INTRODUCTION

Cell migration is a key process during the development of many animal tissues. Much is known about the cues that confer directionality to the migration (Whangbo and Kenyon, 1999; Branda and Stern, 2000; Duchek et al., 2001; Pani and Goldstein, 2018; Szabó and Mayor, 2018; Kim et al., 2019), accuracy in gradient sensing and directionality (Barkai and Leibler, 1997; Endres and Wingreen, 2008), and the signal transduction and cytoskeletal dynamics behind the movement (Abercrombie et al., 1970; Ridley et al., 2003; Svitkina, 2018; van Helvert et al., 2018). In comparison, the termination of migration has been little studied, although it is obviously of key importance for final cell and organ

[1]Institut de Biologie de l'Ecole Normale Supérieure, CNRS, Inserm, 75005 Paris, France. [2]Department of Physics and Astronomy, Purdue University, West Lafayette, IN 47907, USA. [3]Department of Physics and Astronomy, University of Pittsburgh, Pittsburgh, PA 15260, USA.

*Joint first authors

‡Authors for correspondence (felix@bio.ens.psl.eu; andrew.mugler@pitt.edu)

A.M., 0000-0001-9367-7026

position (Meighan and Schwarzbauer, 2007; Aman and Piotrowski, 2010; Inamura et al., 2012; Kikuchi et al., 2015; Paksa et al., 2016). Termination of most cell migrations is thought to be spatially triggered by homogenous concentrations of the guiding cues (Doitsidou et al., 2002), by adhesion to a specific target cell (Rohrschneider and Nance, 2013) and/or by physical barriers (Halfter et al., 2002; Paksa et al., 2016), but was recently shown to be regulated independently of spatial cues, in a time-dependent fashion (Mentink et al., 2014, see below).

The occurrence of cell migration begs the question of the degree of precision in final cell position. The degree of sensitivity of a trait to a given perturbation – or conversely its precision or robustness – is a fundamental characteristic of biological systems (Félix and Wagner, 2008). Although defects in the direction of cell migration are often reported (Burke et al., 2015), few studies have measured the precision in the length of migration and the final position of the cell (Branda and Stern, 2000; Grimbert et al., 2016; Paksa et al., 2016; Lau et al., 2020). Moreover, although the majority of cell migration studies explore the effect of genetic or experimental perturbations, they have not addressed more ecologically and evolutionary relevant types of perturbation, such as environmental, stochastic or natural genetic variation.

The QR neuroblast is a cell that migrates a long distance from the posterior to a more anterior position during the first larval stage of the nematode *Caenorhabditis elegans*. Three rounds of QR cell division take place during or at the end of the migration (Sulston and Horvitz, 1977). The progeny are named according to their anterior or posterior position at each successive cytokinesis: thus, QR.p is the posterior daughter of QR; and QR.pa is the anterior daughter of QR.p. Finally, the daughter cells of QR.pa, called QR.paa and QR.pap (hereafter called QR.pax), acquire a neuronal identity (Chalfie and Sulston, 1981; White et al., 1986) (Fig. 1A,B). Much is known about the signaling pathways, transcription factors and cytoskeleton regulating their posterior-to-anterior direction and orientation of migration (Middelkoop and Korswagen, 2014; Josephson et al., 2016; Rella et al., 2016). Concerning the termination of migration and final cell positioning, the posterior-to-anterior QR.pa lineage stops upon expression of the Wnt receptor MIG-1 (Mentink et al., 2014). Surprisingly, the expression of *mig-1* in QR.pa is not induced by the cell reaching a certain position in the body, but by a temporal regulation, independently of cell position. Indeed, preventing QR migration or increasing its speed does not alter the timing of *mig-1* expression (Mentink et al., 2014). After QR.pa stops migrating, its daughter cells QR.pax separate in a dorso-ventral direction while crossing each other in an antero-posterior direction (Rella et al., 2016; Altun and Hall, 2020); they then differentiate without further change in cell body position.
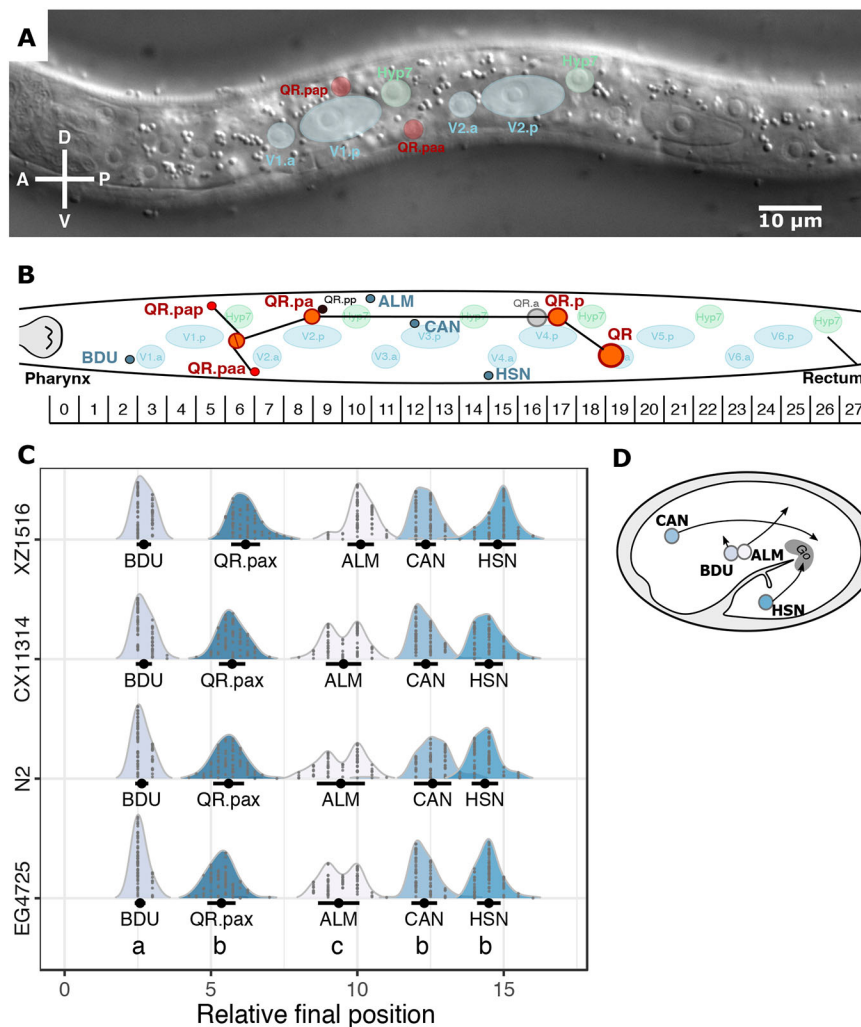
We here probe the sensitivity of this system to various perturbations of ecological and evolutionary relevance. We score both the mean and the distribution of the final cell position.

DEVELOPMENT

1

Fig. 1. QR.p neuroblast migration during the L1 stage and its sensitivity to noise. (A) Nomarski micrograph of a late L1 larva, where QR.pap and QR.paa have reached their final position. The relevant cells are outlined. (B) Illustration of QR.p neuroblast migration during the L1 stage showing the final position of QR.paa and QR.pap, and the relative scale used in scoring their position. The scale from 0 to 27 was constructed relative to the seam cells, as shown here. The positions of BDU, ALM, CAN and HSN neurons in the larvae are also shown. (C) Sensitivity of QR.pax final position to noise. We measured the final position of QR.pax and that of other neurons that migrate, albeit over shorter distances, during embryogenesis: BDU, ALM, CAN and HSN. Black dots and error bars represent the mean±s.d.; n=70 per strain, two replicates merged. a-c represent groups of cells with similar variance (Levene's test for homogeneity of variance). (D) Illustration of BDU, ALM, CAN and HSN migration during embryogenesis (adapted, with permission, from Altun and Hall, 2020).

First, noise, or stochastic variation, is measured by variation in the trait among isogenic animals grown in the same environment (Spudich and Koshland, 1976; McAdams and Arkin, 1997; Elowitz et al., 2002). In our study, we measured the degree of robustness (or sensitivity) of QR.pax final position by comparing its variance with that of other migrating neuronal cell bodies: those of ALMR, BDUR, CANR and HSNR (thereafter called ALM, BDU, CAN and HSN) (Sulston et al., 1983; Hedgecock et al., 1987) (Fig. 1C). These neurons migrate during embryogenesis (Fig. 1D). In *C. elegans*, the Wnt ligand EGL-20 forms a gradient from the tail to the anterior part of the animal and drives QR migration as well as that of HSN. One mechanism for their final positioning is the homogeneous concentration or undetectable level of the guiding cue (attractive or repulsive). Much evidence now shows that HSN stops when EGL-20 concentration is low. More precisely, the location of the CAN neurons defines the final position of HSN (Forrester and Garriga, 1997) by sequestering EGL-20 protein in its vicinity (Modzelewska et al., 2013). As for CAN, BDU and ALM, the mechanism of the final positioning and even the guiding cues are not totally uncovered. CAN neurons are probably guided by several molecular cues at the same time (Silhankova and Korswagen, 2007) and more specifically by EGL-17/FGF signaling (Fleming et al., 2005). The end of their migration may be related to a specific location in the animal at given concentrations of the different molecules. However, a timing mechanism cannot be ruled out for

the final position. Nonetheless, those cells migrate during embryogenesis a much smaller distance than QR. This is another reason to expect a smaller variance in their position compared to that of QR.pax, and thus they constitute a good comparison.

Second, we reasoned that, given the temporal regulation of *mig-1* expression and of the migration endpoint, a change in L1 larva body size would lead to a shift in the final cell position relative to other landmarks along the antero-posterior axis – provided that cell migration occurs at the same speed in animals of different body sizes. The expectation is that, in longer animals, QR.pa stops in a more posterior position relatively to body landmarks, and in smaller animals at a more anterior position. To address the effect of body size on the relative position of QR.pax, we used different body size mutants in the reference genetic background N2. In parallel, we developed a mathematical model of the expected relationship between body size and QR.pax final position, taking into account larval growth during cell migration. We used the fact that body size depends on the age of the mother (Perez et al., 2017) and also measured the effect of the maternal age on body size and QR.pax final position, in N2 and three wild isolates.

Third, we perturbed the external environment in two ways. We first tested the effect of starvation at hatching, before QR migration. After embryonic development inside its egg shell, *C. elegans* hatches in the first larval stage (L1) in the shape of a small worm. If no food is provided, the larva enters a developmental arrest program that can last

for several days, prior to QR migration and first division (Johnson et al., 1984; Baugh, 2013). QR migration starts shortly after feeding the animal. We thus tested the robustness of QR.pa final position to this temporary developmental arrest after hatching. Then, we tested the effect of an environmental perturbation that is highly relevant in the wild, namely different temperatures, from 15°C to 25°C. We performed these two experiments controlling for the maternal age.

Fourth, we explored natural variation using a panel of *C. elegans* wild isolates. The study of wild isolates reveals natural variation for phenotypic traits (Hodgkin and Doniach, 1997; Farhadifar et al., 2015; Cook et al., 2016; Gimond et al., 2019; Lee et al., 2019) and different genotypes can reveal different sensitivities to perturbations (Braendle and Félix, 2008). So far, QR.pax final position had only been measured in the laboratory-evolved reference background N2 and mutants from this strain. Laboratory adaptation may alter many phenotypes in many organisms, including *Drosophila melanogaster* (Stanley and Kulathinal, 2016), *Caulobacter crescentus* (Marks et al., 2010) or *Caenorhabditis elegans* (McGrath et al., 2009; Sterken et al., 2015). We therefore wondered to what extent the final position of QR.pax evolved within *C. elegans*; and whether the degree of robustness to noise and environmental perturbations was a shared feature between laboratory-adapted genotypes and wild isolates.

We find that the variance of QR.pax final position is similar to that of other neurons that migrate at a long-range during embryogenesis. Moreover, as expected from the temporal mechanism of migration termination, smaller mutants display more anterior QR.pax cells, whereas longer mutants and tetraploids display posteriorly shifted QR.pax cells. Progeny from 1-day-old mothers are also smaller and exhibit a significantly more anterior QR.pax final position. A starvation treatment at hatching increased the variance of QR.pax, whereas at higher temperatures its mean position undergoes a posterior shift, showing that the system is not fully robust to external perturbations. Finally, we could detect highly significant variation among *C. elegans* wild isolates that was not significantly explained in our tested panel by variation in body size.

RESULTS
Variance in QR.pax final position is similar to that of other migrating neurons
The sensitivity to noise, or stochastic variation, is measured by the variance of a trait in a population of isogenic individuals in a constant environment. Using N2 and three genetically distinct wild isolates, we first compared the variance in QR.pax final position with that of other neurons that migrate during embryogenesis: BDU, ALM, CAN and HSN (Sulston et al., 1983; Hedgecock et al., 1987) (Fig. 1C). The cell body position of these neurons can be measured in the same animals with the same scale as that of QR.pax, using epidermal cell landmarks (Harris et al., 1996; Forrester and Garriga, 1997; Ch'ng et al., 2003; Zinovyeva and Forrester, 2005; Zinovyeva et al., 2008) (see Materials and Methods). The variance in QR.pax final position is similar among the four strains (F=0.48, P=1) and the two replicates (F=0.15, P=1) but not among the six neurons (F=37.8, $P<10^{-15}$). BDU has significantly lower variance than the other migrating neurons, which likely reflects the fact that it only migrates a short range. The variance of QR.pax is similar to those of CAN (F=5.5, P=0.19) and HSN (F=4.4, P=0.36). ALM has a slightly larger variance than the other neurons ($F>9$, $P<0.02$). Altogether, this result reveals that QR.pax final position is quite robust to noise, despite the temporal regulation of its migration endpoint. Among wild isolates, we do not observe consistent co-variation between migrating neurons, except for QR.paa and QR.pap (Table S1). This also implies that using QR.pax as the mean position between QR.paa and QR.pap is relevant.

QR.pax final position is sensitive to body size
The end of QR.pa migration relies on the timing of expression of *mig-1* and not the position of the cell in the animal (Mentink et al., 2014). From this observation, we can predict that body size affects QR.pax final position: in a longer body, the cell should stop at the same time, i.e. at a more posterior position; conversely, in a shorter body, the cell should stop at a more anterior position (Fig. 2A, left). Alternatively, body size variation may be fully compensated and the relative position of QR.pax remains unchanged at various body sizes (Fig. 2A, right).

We thus tested whether body size affects QR.pax position. We selected a set of mutants in the N2 reference background with a smaller or a longer egg size and without general cell migration defect (Fig. S1A). These include mutants in four genes as well as tetraploid animals with an overall larger body size [*C. elegans* is normally diploid (Nigon, 1951a)]. *larp-1* encodes a La-related protein. A loss of function of this gene upregulates Ras-MAPK during oogenesis, leading to smaller oocytes (Nykamp et al., 2008). The loss of function of *sma-1*, encoding a βH-spectrin, impairs embryonic elongation and leads to smaller body size (McKeown et al., 1998). *lon-1* encodes a cysteine-rich secretory protein (CRISP). Loss of function of this gene results in the upregulation of the TGFβ pathway, increasing body size by hypodermal endoreduplication, observed in the adult stage (Morita et al., 2002). It also may affect egg length by physical compression in the gonad arm (Yamamoto and Kimura, 2017) but its effect on early larval development was not studied. *fln-1* encodes a filamin required for proper ovulation (Kovacevic and Cram, 2010). Nonetheless, how the loss of function allele *fln-1(ok2611)* affects egg and L1 length is unknown.

In these mutants, we measured QR.pax final position and found that, in *lon-1* (t=2.8, P=0.03), *fln-1* (t=5.7, $P<10^{-6}$) and tetraploid (t=17.7, $P<10^{-35}$) animals, the final position of QR.pax was significantly more posterior than that in N2. The smaller *larp-1* (t=−3.2, P=10^{-2}) and *sma-1* (t=−2.64, P=0.05) animals exhibited a more anterior QR.pax position (Fig. S1B).

To quantify the correlation between body size and QR.pax final position, we then measured pharynx-to-rectum (P-to-R) distance at hatching and 6 h after hatching. We first found that the P-to-R distance at hatching and 6 h after hatching were correlated with egg length in N2 and its different mutants (Fig. S1C,D). Most importantly, the empirical measurements revealed that QR.pax final position and P-to-R distance were correlated (Fig. 2B), with longer animals having a more posterior QR.pax relative position. QR.pax position was also correlated with egg length and P-to-R distance 6 h after hatching (Fig. S1F,G). This indicates that, as expected from the temporal regulation of its migration endpoint, QR.pax final positioning is sensitive to body size.

We established a mathematical model of the expected final position of QR.pax as a function of body size. The larva grows during the cell migration, as measured in Table S1, which is taken into account in the model (see Materials and Methods). The model predicts the relationship between QR.pax position and body size at a given timepoint, in the absence of compensation (Fig. 2C, red curve). Compared with the best-fit model without body size compensation, the empirical measurements show an effect on body size on QR.pax position that is smaller than that predicted by this simple model version, indicating the presence of a partial compensation mechanism.

We investigated two different scenarios of partial compensation to decipher the relationship between body size and QR.pax final position: an adaptation of the duration of migration of QR.p (but not
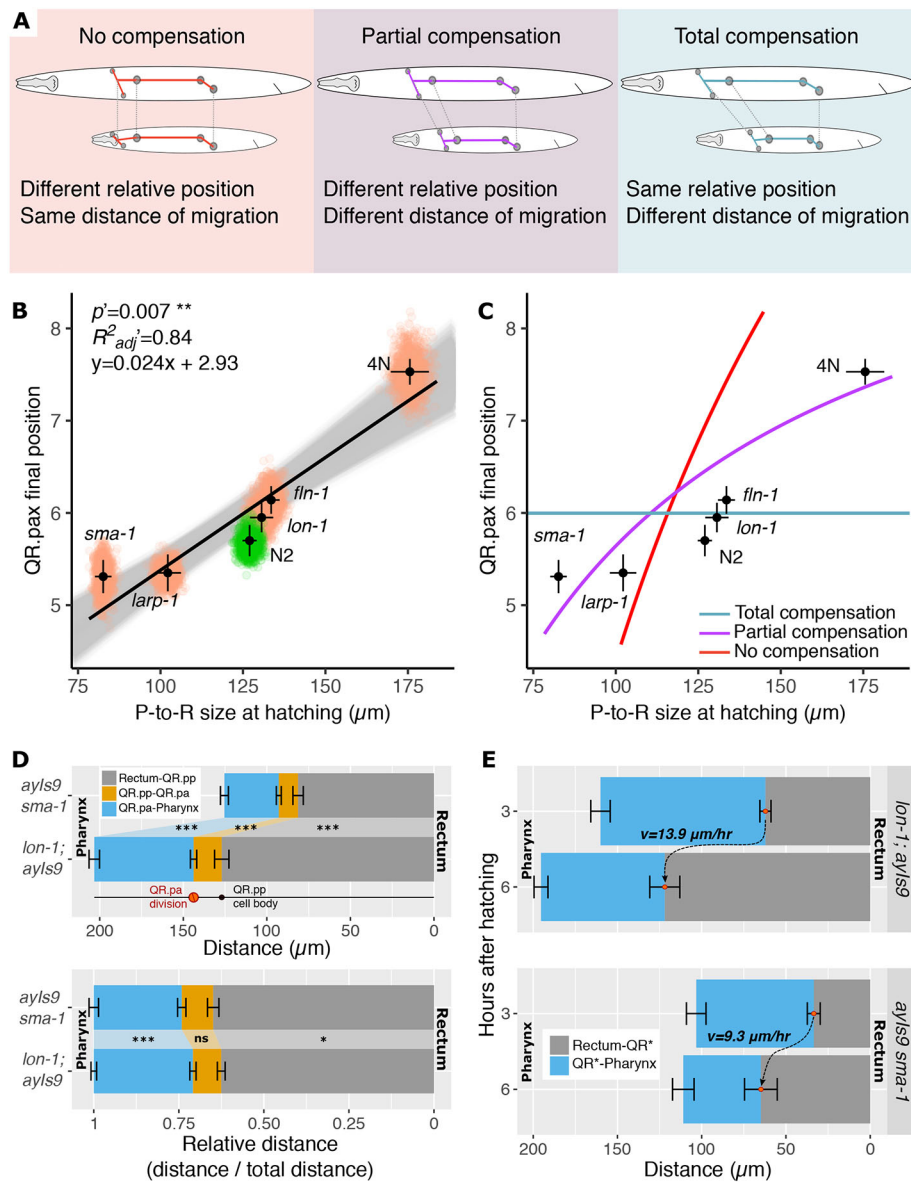
Fig. 2. Sensitivity of QR.pax position to body size using mutants in the N2 background. (A) Schematics of the relative position of QR.pax in a long versus a short animal in the absence of body size compensation (left), with full compensation (right) or with a partial compensation (middle). (B) Relationship between QR.pax final position and pharynx-to-rectum distance at hatching in a subset of the panel. Orange and green dots represent one round of subsampling of the data. Black dots and error bars represent the mean±confidence intervals (c.i. 95%) from the data for each genotype. The black line represents the regression line from the data. The grey area represents regression lines after each iteration of subsampling. (C) Mathematical model of the relationship between QR.pax final position and pharynx-to-rectum distance assuming full body size compensation, no compensation (with one fit parameter, cell velocity) or partial compensation (with no fit parameters). (D) Location of QR.p and QR.pa divisions in *ayIs9 sma-1* and *lon-1; ayIs9* backgrounds, in absolute value of distance to the rectum and pharynx or scaled relatively to body size. The apoptotic body of the QR.pp cell marks the site of QR.p division. Bars and error bars represent the mean and confidence intervals (95%) per genotype; *n*>20 per strain. Two-sided *t*-test: ***$P<0.001$, *$P<0.05$, n.s., not significant. (E) Absolute distances between the rectum, QR* cell and the pharynx 3 and 6 h after hatching in *lon-1; ayIs9* and *ayIs9 sma-1* animals. At 3 h QR* is either QR or QR.p in some animals; at 6 h QR* is either QR.p division or QR.pa in *lon-1; ayIs9* and mostly QR.p in *ayIs9 sma-1*. Bars and error bars represent the mean±c.i. (95%) per genotype; *n*≥10 per genotype. The cell velocity *v* was calculated using Eqn 9.

QR.pa) to body size or an adaptation of the cell velocity to body size. In the first case, given that the temporal regulation of *mig-1* expression occurs at the end of the migration, we hypothesize that body size would affect the last part of the migration only, i.e. the short-range migration of QR.pa. Thus, the relative position of QR.p division should be similar between long and short animals. Measurements of the QR.p site of division (Rectum to QR.pp) and QR.pa site of division (QR.pp to QR.pa) did not support this hypothesis (Fig. 2D), as the relative position of QR.p division is more anterior in small animals ($t=-2.4$, $P=0.02$). In the second scenario, one can predict a mechanism through which the cell velocity is adapted to the body size, where the cell migrates faster in long animals. To estimate cell speed at different body sizes, we used the *sma-1* and *lon-1* mutants (the latter is close in body size to the wild-type N2; Fig. 2B). We measured cell position at two timepoints during migration (t=3 h after hatching and t=6 h after hatching) and inferred cell velocity through the mathematical model, taking into account larval growth (Eqn 9). We found that the migration speed of the QR lineage from 3 h to 6 h after hatching was higher in *lon-1(e185); ayIs9* mutants (13.9 µm/h) compared with *ayIs9 sma-*

1(e30) mutants (9.3 µm/h) (Fig. 2E). These results are consistent with a partial compensation mechanism of body size acting on cell velocity. Indeed, incorporating these data into the model provides a good fit to the measurements, using no free parameters (Fig. 2C, purple curve).

Another way in which to assess the sensitivity to body size, within a genotype, was to take into account the effect of maternal age. As previously shown by Perez et al. (2017), we found that progeny from 1-day-old mothers were smaller than those from day 2 ($Z=5.87$, $P<10^{-4}$) and day 3 ($Z=7.03$, $P<10^{-4}$) (Fig. 3A). The difference between day 2 and day 3 was not significant ($Z=1.16$, $P=0.48$). As expected if body size affects QR.pax final position, the progeny from day 1 mothers exhibited a more anterior position compared with progeny from day 2 ($Z=2.54$, $P=0.03$) and day 3 ($Z=3.46$, $P=0.002$) mothers (Fig. 3B). The impact of the maternal age on QR.pax final position, even if significant, is minor when compared with the genotype effect. The difference between day 2 and day 3 was not significant ($Z=0.92$, $P=0.63$). Using these maternal age results, we find a correlation between QR.pax final position and pharynx-to-

DEVELOPMENT
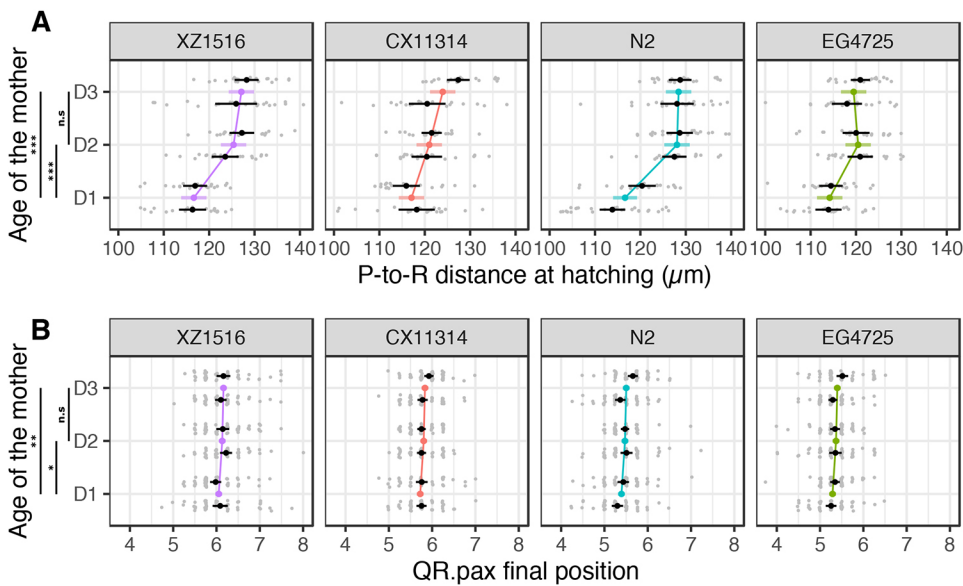
Fig. 3. Effect of the maternal age on body size at hatching and QR.pax final position. Pharynx-to-rectum distance at hatching (A) and QR.pax final position (B) were measured in the same population of progeny of 1- (D1), 2- (D2) and 3- (D3) day-old hermaphrodites. Grey dots represent the P-to-R distance at hatching and QR.pax final position of each animal; black dots and error bars represent the mean±c.i. (95%) of the two replicates: the colored dots and error bars represent the mean±c.i. (95%) of the fitted value estimated with the linear mixed model. n=50 per strain, temperature and replicate, ***P<0.001, **P<0.01, *P<0.05, n.s., not significant.

rectum distance at hatching for each of the four tested strains (Fig. S2). The maternal age may also influence QR.pax final position independently of the body size.

Early developmental arrest affects the variance of QR.pax, while temperature affects its mean position

We tested two ecologically relevant environmental variables for their effect on QR.pax positioning: starvation at hatching and different growth temperatures. After hatching in the absence of food, larvae of *Caenorhabditis elegans* stop their development, a phenomenon known as the L1 arrest, which is regulated by insulin signaling (Kaplan and Baugh, 2016; Zheng et al., 2018). We used two methods to assess the sensitivity of QR.pax to starvation. The first one involved selecting for bleach-resistant embryonic stages by bleaching 1- or 2-day-old hermaphrodites and letting the larvae hatch without food for 40 h. The second method consisted of letting the population grow and consume all bacteria, leaving the recently hatched larvae without food for 48 h. In each case, we then provided them with food and scored them 6-8 h later, once QR.paa had reached the ventral part of the animal, QR.pap had reached the dorsal part (and thus both had stopped their migration) and the V seam cells had divided once. We found with the first method that the variance was similar for the four strains when fed (F=0.80, P=1 from day 1 offspring of hermaphrodites and F=1.99, P=0.35 from day 2) or when starved (F=0.20, P=1 from day 1 offspring of hermaphrodites and F=1.04, P=1 from day 2). Nonetheless, starvation increased considerably the variance compared with continuously fed worms (F=10.62, P<10^{-10} from day 1 hermaphrodites' offspring and F=10.51, P<10^{-10} from day 2) (Fig. 4A). We found similar results when we used a more ecologically relevant method of food deprivation without bleaching; however, this does not control for maternal age (Fig. S3A). After L1 starvation, the variance of other neurons does not seem to be largely altered, especially in the XZ1516 strain (Fig. S3B).

Temperature can affect various developmental processes in the embryo and the larva. Plates containing L1 larvae were transferred from 20°C to different temperatures (15°C, 20°C or 25°C) one generation before scoring. The same four strains were scored as above. The factor with the strongest effect on final position is the

genotype (X^2=364.28, P<10^{-15}). A lower temperature shifts QR.pax to a more anterior position (X^2=141.10, P<10^{-15}). The strength of this effect is also modulated by the genotype (genotype×temperature interaction: X^2=12.51, P=0.006) (Fig. 4B). The temperature shifts QR.pax final position toward the anterior as the temperature decreased, with a value of 0.054 relative position unit per degree in the genetic background N2. This value decreases to 0.046 in the strain CX11314, to 0.030 in XZ1516 and to 0.025 in EG4725. We found similar results in an experiment where the age of the mother was not controlled (Fig. S3C, Table S1).

Differences in final cell position may result in downstream differentiation phenotypes, such as variation in axon morphology in the case of neurons. QR.paa becomes the AVM mechanosensory neuron. We thus monitored axons of mechanosensory neurons after starvation of GOU174 (genotype *casIs35*; *zdIs5*), a strain exhibiting a GFP reporter in mechanosensory neurons, including AVM (see Materials and Methods). We scored larvae at the L3 stage and used the AVM cell body as a landmark. In these conditions, the variance of AVM is also higher after starvation in the L3 stage compared with the control (F=22.6, P<10^{-5}) (Fig. S4A). Out of 200 animals in each condition, we only observed three animals with defects in axon (defasciculation, hook or extra branching) in the control population and also three after starvation. Axon formation is thus robust to early starvation and differences in cell position. In the wild-type condition, the PLM projection stops posteriorly to AVM and ALM (Fig. S4B). Nonetheless, we found that the AVM cell body (Fig. S4C) or projection (Fig. S4D) was more frequently in the vicinity of PLM projection after starvation (*LR* X^2=16.8, P<10^{-4}). An overlap between PLM projection and ALM has been previously observed in *sax-1* and *sax-2* mutants (Gallegos and Bargmann, 2004) but the overlapping between PLM and AVM was not discussed. More interestingly, we found that this close proximity (overlapping) is more prone to appear when AVM is posterior (*LR* X^2=22.9, P<10^{-5}) (Fig. S4A).

Natural variation of QR.pax final position in wild isolates

QR.pax position has been studied only in the laboratory-adapted genetic background N2. The occurrence and span of natural variation for this trait was unknown. Above, we detected natural

DEVELOPMENT
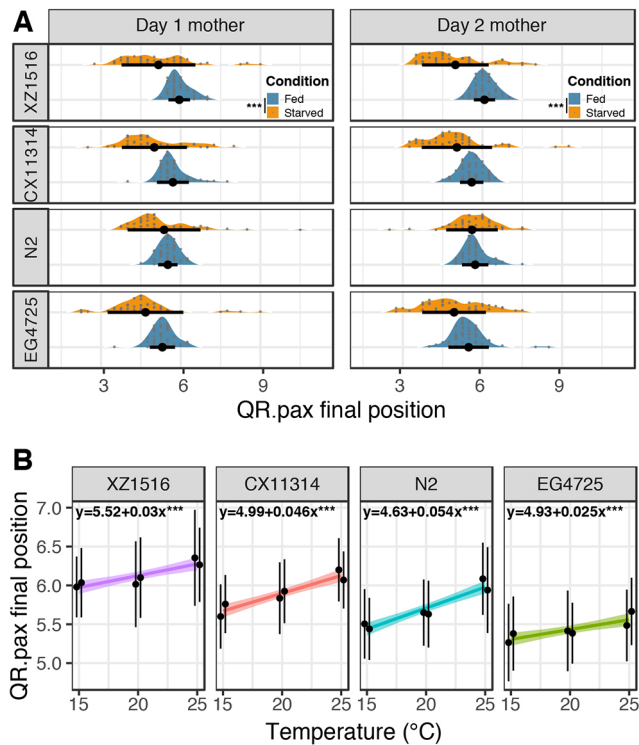
Fig. 4. Sensitivity of QR.pax to environmental variations. (A) Sensitivity of QR.pax to a starvation treatment in the L1 stage. Day 1 mothers and day 2 mothers were bleached and embryos transferred to culture plates with or without *E. coli* food. Arrested larvae were kept starved for 40 h before being fed again and allowed to develop. Day 1 mother and day 2 mother experiments were conducted and analyzed separately. Black dots and error bars represent the mean±s.d.; *n*=40 for starved larvae and *n*=50 for fed larvae per strain and condition. Levene's test for homogeneity of variance: ***P<0.001. (B) Robustness of QR.pax to temperature. One-day-old mothers were transferred from 20°C to either 15°C, 20°C or 25°C, and allowed to lay eggs for 7 h before being removed. Larvae were scored the next day when QR.pax has stopped moving. Black dots and error bars represent the mean±s.d. of each replicate; the colored lines represent the regression line with the associated equation estimated with a linear mixed model. *n*=50 per strain, temperature and replicate (***P<0.001).

variation among the four tested strains (Figs 1D, 3B and 4A,B). We further measured QR.pax final position in a panel of 40 *C. elegans* strains (N2 and 39 wild isolates) that is representative of the genetic diversity of the species (Cook et al., 2017). We observed natural variation in QR.pax final position among the wild isolates (Fig. 5A, F=18.9, P<10^{-15}). The mean value of QR.pax final position in the N2 background is close to the grand mean in the species. Some isolates revealed a more-anterior position (such as ECA36 and CB4932) and others a more posterior position (such as XZ1516 and JU830) (Fig. 5B).

Considering the sensitivity of QR.pax final position to body size, we wondered whether natural variation in QR.pax position was explained at least partially by variation in body size. We measured egg lengths, larval lengths (P-to-R distances) at hatching and 6 h after hatching in a subset of 14 strains. We performed one experiment in progeny coming from day 2 mothers and one experiment without controlling the maternal age. We found in the day 2 mother experiment a correlation between egg length, P-to-R distance at hatching and 6 h after hatching (Fig. S5A-C). These correlations were obscured in the experiment where maternal age was not controlled (Fig. S6A-C).

Interestingly, we did not find any significant correlation between QR.pax final position and body size in this set of isolates, in both experiments, suggesting that body size did not explain the variation in QR.pax final position and was thus compensated for during evolution of the *C. elegans* species (Fig. 5C, Figs S5D,E and S6D-F). Strangely, QR.pax final position appears to be marginally correlated with egg length (although not to larval length) in the two independent experiments (Figs S5D and S6D). This weak correlation may be spurious, or else explained by the genetic variation among isolates acting pleiotropically on the two phenotypes.

As the temperature of growth affects the final position of QR.pax, we wondered whether the temperature of origin of the wild isolates could explain a part of the natural variation. The only information available is the latitude and longitude of the sampling location. We used the sampling latitude (in absolute value) of each strain as a proxy for the natural habitat temperature. We did not find a correlation between QR.pax final position and the absolute value of the sampling latitude (t=-0.94, P=0.35).

DISCUSSION
Variance in final cell position
To determine whether the temporally regulated position of QR.pa daughters is sensitive to various perturbations, we used different types of metrics. (1) For most measurements, we used a scale that takes as landmarks the lateral epidermal seam cells, as widely used in studies of QR/QL positioning (Coudreuse et al., 2006; Harris et al., 1996; Mentink et al., 2014; Whangbo and Kenyon, 1999). Although nematodes are not segmented, their organization is formed of repeats along the antero-posterior axis, particularly strikingly of these lateral epidermal seam cells. In our scale, each such repeat along the antero-posterior is further divided in four units, with a total of 27 units between the base of the pharynx to the rectum (Fig. 1B). QR is born before hatching as the sister of the lateral epidermal seam cell V5R and therefore its starting point is always the same on this scale (Sulston et al., 1983; Hedgecock et al., 1987). (2) In some cases, we measured cell position in micrometers from the base of the pharynx or from the rectum (e.g. Fig. 2D,E). (3) When we varied body size, we scaled the micrometer measurements to a body length measurement (e.g. Fig. 2D).

We find that the variance in QR.pax position, as well as the observed range, stay within the length of a repeat along body length (four of our scale units). The range encompasses about half a repeat length (two scale units). However, after starvation in the L1 stage, the observed range encompasses over a repeat length. Comparing with better known examples from other model organisms, this range of QR.pax sensitivity to stochastic noise in the starvation treatment would correspond to the antero-posterior displacement of an insect appendage to the next segment, which would be considered a dramatic transformation. In this starvation experiment, we only scored animals where development of seam cells and the QR lineage was not strongly retarded (see Materials and Methods) and thus the range may be even greater if all animals were considered. The increase in variance may be explained by the fact that after a long L1 starvation period, the growth rate of the worms is affected and development is delayed (Lee et al., 2012). This delay can potentially affect the timing of V seam cell division (Olmedo et al., 2020) as well as the intrinsic dynamics of QR migration. It has been shown that a supplement of cholesterol promotes QR migration and division on arrested larvae (Qu et al., 2020). The presence of cholesterol in the NGM might provide another possible explanation of QR migration in starved worms (see Materials and Methods).

DEVELOPMENT
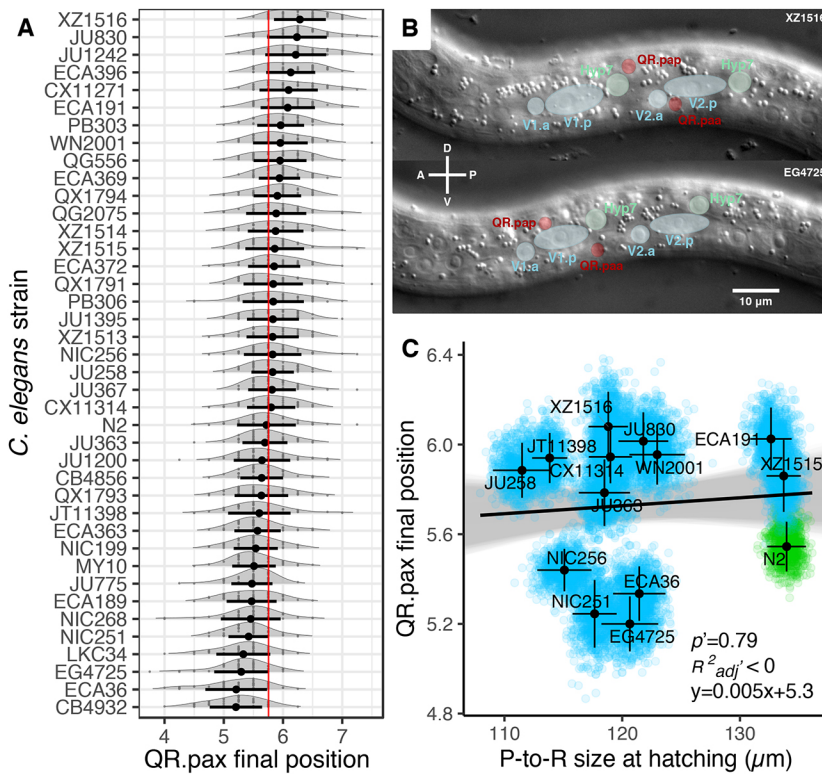
Fig. 5. Natural variation of QR.pax final position in *C. elegans*. (A) Natural variation of QR.pax final position in a panel of 40 *C. elegans* wild isolates. Grey dots represent QR.pax final position for each animal; black dots and error bars represent the mean±s.d. per genotype, respectively (*n*=50 per strain). The red line indicates the grand mean over the 40 isolates. (B) Nomarski micrograph of late L1 larvae showing an example of posterior (strain XZ1516, top) and an anterior (strain EG4725, bottom) QR.pax relative position. (C) Relationship between QR.pax final position and pharynx-to-rectum distance at hatching in a subset of the panel, from 2-day-old mothers. Blue and green dots represent the mean after one round of subsampling. Black dots and error bars represent the mean±c.i. (95%) for each genotype from the data. The black line represents the regression line from the data. The grey area represents regression lines after each iteration of subsampling.

Importantly, the fact that BDU, ALM, CAN and HSN positions are not affected by early starvation also suggests that the relative scale used to measure the final position is not impaired by this treatment.

Concerning growth temperature, many biochemical and thus developmental processes are likely to be affected, including embryo size and the growth rate of the larva (Gutteling et al., 2007). At high temperature, the posterior position of QR.pax might reflect the fact that the growth rate of the larvae is increased but not QR migration. The gene expression profile also varies with temperature (Gómez-Orte et al., 2017). Another hypothesis is that a higher temperature can lead to a precocious (or higher) expression of *mig-1*, thus stopping QR.pa migration earlier. The diversity of reactions that may be affected by temperature makes it difficult to make hypotheses regarding the mechanism.

To some extent, displacements in the final position of the cell body can be compensated for. For example, in neurons, axon growth can be modulated according to the distance to the target by cell extrinsic determinants (Hekimi and Kershaw, 1993). Nonetheless, in other cases, a shift in the position of neuronal cell bodies can drastically alter their fate and morphology (Martineau et al., 2018). We wondered whether changes in the final position of QR.pax lead to differences in downstream neuronal phenotypes. We observed that posteriorly shifted AVM tends to be in the vicinity of the PLM projection after early starvation. We do not know whether a synaptic connection is established between these two mechanosensory neurons and whether this may be (counter)selected.

A model without free parameters suggests partial compensation of body size

We observed that cells migrate farther in the animal relative to landmarks when body size is small, and less far when it is large. This observation is qualitatively consistent with the fact that these cells stop after a certain amount of time: if the speed is constant, they will migrate a constant distance, which will be larger relative to a

smaller body. However, quantitatively, the degree of this effect was observed to be less than predicted by the model, even for the best-fit value of the constant speed. Indeed, in absolute values (micrometers), cells migrate farther when body size is large, and less far when body size is short (Fig. 2C). We therefore hypothesized that partial compensation may be acting through a change in cell speed as a function of body size, i.e. if QR and its progeny migrate faster at larger body size. To test this hypothesis, we measured cell speed in *sma-1* versus *lon-1* mutants (Fig. 2D) and using the model, we indeed found that the partial compensation of body size did operate through a change in cell speed. The improved model provided a quantitatively accurate description of the measurements. Moreover, given the known inputs (cell start position, cell start and stop time, cell velocity in two mutants and larval growth speed), the improved model succeeded with no fit parameters.

Our mathematical model is minimal in its construction yet quantitatively accounts for the observations. Some simplifying assumptions are supported by the data, e.g. the observation that all larvae, independent of mutant strain, grow a constant amount in 6 h. We have checked other assumptions explicitly; e.g. we find that the results are negligibly changed if the cell accelerates and decelerates instead of instantaneously starting and stopping its migration. This result also suggests that our results would be unaffected by details such as temporal variations in cell speed or pauses due to cell division.

Possible mechanisms of cell speed dependence on body size could be the following. First, migration speed could be increased at larger cell size. Nonetheless, evidence from the literature tends to associate a negative correlation between cell size and cell velocity *in vitro* under adhesive conditions (Leal-Egaña et al., 2017; Hennig et al., 2020). Second, body size could affect extracellular matrix density, such that larger cells secrete a less tight matrix, resulting in faster net migration speed, as in the *emb-9* matrix collagen mutant

DEVELOPMENT

(Kawano et al., 2009; Mentink et al., 2014). Third, body size could affect the properties of the Wnt gradient influencing QR migration; this could operate if, for example, a larger body size resulted in stronger Wnt concentrations at a given relative position, resulting in faster cell speed (Mentink et al., 2014). Finally, it is possible that the cell speed modulation mechanism depends upon the specific mutants we used for these assays.

Natural variation

All previous studies of QR migration were performed in the laboratory-modified N2 background of *C. elegans*. Here, we uncover variation in the final position of QR.paa and QR.pap when exploring a representative set of *C. elegans* wild isolates. The variance in QR.pax position appears similar in all isolates but the mean position differs from about 1/4 of a body repeat (1 on our measurement scale) from CB4932 to XZ1516 (Fig. 5A) in standard laboratory conditions. When considering different individuals, QR.pax position may vary in a range of almost a full body repeat among different individuals of different wild genotypes (3.75-7.5 on our scale; see Fig. 5B for such representative animals).

Body size variation in the L1 stage is substantial among wild isolates, and almost covers the range of the body size mutants we used, excluding the tetraploid animals. However, we did not find a correlation between QR.pax body position and L1 body size in the subset of wild isolates we used for this analysis. This may be due to a lack of power or may suggest the presence of an evolutionary compensation in QR.pax position relative to body size variation. QR velocity and its migration dynamics can be affected in a different manner in each isolate. In any case, we conclude that natural variation in QR.pax position is not fully explained by body size variation. The available natural variation in QR.pax position will allow us in the future to analyze the genetic basis for the observed natural variation in the final position of a long-range migrating cell.

MATERIALS AND METHODS
C. elegans strains

Caenorhabditis elegans were grown at 20°C on 55 mm diameter Petri dishes with NGM, fed on *Escherichia coli* OP50 according to the standard procedures (Brenner, 1974). To investigate the relationship between body size and QR.pax final position, we selected a list of mutations in the reference genetic background N2 known to affect egg size and *a priori* not cell migration: JJ1271 *glo-1(zu391)* (Hermann et al., 2005), GL302 *cid-1(rf34)* (Olsen et al., 2006), RB2488 *amph-1(ok3443)* (The C. elegans Deletion Mutant Consortium, 2012), RB1658 *mca-3(ok2048)* (The C. elegans Deletion Mutant Consortium, 2012), BA819 *spe-11(hc77)* (L'Hernault et al., 1988), GH383 *glo-3(zu446)* (Rabbitts et al., 2008), JT513 *nrf-5(sa513)* (Choy and Thomas, 1999), JT73 *itr-1(sa73)* (Iwasaki et al., 1995), RT362 *rme-4(b1001)* (Sato et al., 2008), JK4545 *larp-1(q783)* (Nykamp et al., 2008), CB30 *sma-1(e30)* (Brenner, 1974), RB1977 *fln-1(ok2611)* (The C. elegans Deletion Mutant Consortium, 2012), CB185 *lon-1(e185)* (Brenner, 1974) and the tetraploid 4A:4X strain SP346 (Madl and Herman, 1979).

To investigate the natural variation for the trait, we used the following wild isolate strains (Cook et al., 2017): CB4856, CB4932, CX11271, CX11314, ECA189, ECA191, ECA36, ECA363, ECA369, ECA372, ECA396, EG4725, JT11398, JU1200, JU1242, JU258, JU363, JU367, JU775, JU830, JU1393, LKC34, MY10, NIC199, NIC251, NIC256, NIC268, PB303, PB306, QG2075, QG556, QX1791, QX1793, QX1794, WN2001, XZ1513, XZ1514, XZ1515 and XZ1516.

The strain NH646 *ayIs9[Pegl-17::gfp+dpy-20(+)]; dpy-20(e1282ts)* (Branda and Stern, 2000) with a Q lineage GFP reporter was also used in this study (a kind gift from the Korswagen laboratory, Hubrecht Institute, Utrecht, The Netherlands). The strain GOU174 *casIs35[Pgcy–32::mCherry, unc–76(+)] X; zdIs5[Pmec–4::gfp, lin–15(+)]I* (Zhu et al., 2016) was used to observe cell body and axon of mechanosensory neurons, including AVM (QR.paa) (a kind gift from the Ou laboratory, Tsinghua University, Beijing,

China). To visualize the Q lineage in body size mutants, we generated the strains JU4128 [genotype *ayIs9 sma-1(e30)*] and JU4129 [genotype *lon-1(e185); ayIs9*] by crossing NH646 males carrying the *ayIs9[Pegl-17::gfp+dpy-20(+)]* transgene with hermaphrodites of strain CB30 carrying *sma-1(e30)* and of strain CB185 carrying *lon-1(e185)*, respectively.

QR.pax final position measurements in N2 mutants and wild isolates

QR.paa and QR.pap final positions were measured using Nomarski microscopy of late L1 larval stage animals mounted on 3% agar pads and immobilized with 1 mM sodium azide. At this stage, the V seam cells have divided once, QR.paa has reached its final ventral position and QR.pap its final dorsal position in the animal. QR.pax final position is the mean position of QR.pap and QR.paa in each individual, measured with a relative scale based on the V-derived seam cells (Harris et al., 1996; Whangbo and Kenyon, 1999; Coudreuse et al., 2006; Mentink et al., 2014). The relative position of QR.paa to QR.pap does not change when the long-range migration of their ancestors is affected (Mentink et al., 2014). We constructed a semi-discrete scale from the pharynx (0) to the rectum (27), based on the repeated pattern formed by the nuclei of the seam cells and hyp7 cells. A half value is attributed when the nucleus is between two landmarks. In some cases, we also measured distances in micrometers.

Robustness to noise

We measured the variance of QR.pax position when faced with stochastic noise and compared it with that of other neurons migrating during embryogenesis: BDU, ALM, CAN and HSN (Sulston et al., 1983; Hedgecock et al., 1987). These neurons are easily recognizable and are in the same environment as QR.pax. We could use the same relative scale to measure the position of the bodies of these cells and compare variance between them. We performed a Levene's test for equality of variance to measure the differences of variance between strains and cell positions, adjusted with Bonferroni correction for multiple testing. The experiment was performed in two replicates and those were merged as there was no replicate effect on the variance (see Table S1).

Distance measurements

We first measured egg length in a set of mutants with a putatively altered embryo size (see list above) and compared their size with that of N2 using a two-sided *t*-test with Bonferroni adjustment of the *P*-value for multiple comparisons. Most body size mutants affect larval growth and not earlier stages. Live embryos of *cid-1(rf34)*, *glo-3(zu446)*, *itr-1(sa73)*, *mca-3(ok2048)*, *rme-4(b1001)* and *spe-11(hc77)* mutants did not show significant differences in length compared with N2 and were thus rejected (Fig. S1A).

We measured QR.pax final position in the remaining mutants with significant differences in egg size. Three mutants had gross defects and we decided to discard them further from the analysis: *amph-1(ok3443)* and *nrf-5(sa513)* exhibited several defects, including cell migration defects for BDU, ALM and/or dorsal-ventral migration of QR.paa and QR.pap; *glo-1(zu391)* mutants had long eggs but small and sick larvae. We then compared QR.pax final position of the mutants to N2 with a two-sided *t*-test and *P*-values were adjusted with the Bonferroni method for multiple comparisons.

To test the correlation between egg size and L1 larva body size, we measured the distance between the rectum and the end of the pharynx, which corresponds to the area of migration of the QR neuroblast from 27 to 0 in our relative scale. Plates containing eggs were washed several times and transferred onto a fresh plate in order to only keep unhatched embryos. Freshly hatched larvae (0-20 min) were mounted on agar pads immobilized with 1 mM sodium azide and measured from the pharynx to the rectum, or transferred to fresh plates to perform the measurements 6 h after hatching.

To test whether body size differentially affected each step of the migration, we measured the distance between the rectum, QR.pp (QR.p site of division), QR.pa and the pharynx, in worms where QR.pa had just divided and the QR.pp apoptotic body was still present. The strains JU4128 of genotype *ayIs9 sma-1(e30)* and JU4129 of genotype *lon-1(e185); ayIs9*

were used to estimate cell velocity of QR by measuring the distance between the rectum, the QR lineage and the pharynx at 3 h and 6 h after hatching, corresponding to QR.p lineage long-range migration. The position of the cell and its stage in the migration cannot be perfectly synchronized between animals so we use the term QR* to designate QR or its progeny. At 3 h QR* represents either QR or QR.p in some animals, at 6 h QR* represents either QR.p division or QR.pa in *lon-1; ayIs9* and mostly QR.p in *ayIs9 sma-1*.

To investigate the effect of QR.pax final position on neuronal differentiation phenotypes, we applied the starvation protocol described above to the strain GOU174 (genotype *casIs35[Pgcy–32*::mCherry, *unc–76(+)*] X; *zdIs5[Pmec–4*::gfp, *lin-15(+)*]I) with a GFP marker for mechanosensory neurons and monitored the axons of AVM (QR.paa), PVM, ALM and PLM. We measured the relative position of AVM by dividing the pharynx-to-AVM distance by the pharynx-to-ALM distance. We measured AVM position in the L3 stage, 31 h after food provisioning to starved worms, with two independent replicate experiments. The control population was obtained by washing plates with M9 to retain only those embryos on NGM. The embryos were then allowed to hatch and feed on OP50 for 41 h before phenotyping. We performed a Levene's test for equality of variances to measure the effect of starvation on the variance in AVM relative position in each replicate and in the whole dataset. The effect of starvation and AVM final position on the axon overlapping phenotype was analyzed with a generalized linear model. The experiment was performed in two replicates and those were merged as there was no replicate effect (see Table S1). Photography and measurements were carried out using a Photometrics CoolSNAP ES camera (Roper Scientific) and software Nikon NIS element D (version 3.1). The size in pixels was then converted to micrometers after calibration [Size (µm)=Size (px)/9.84].

Relationship between QR.pax final position and distance measurements
We used the data of egg length, pharynx-to-rectum distance (hereafter called P-to-R) at two timepoints (0 and 6 h) and QR.pax final position of each strain to test relationships between these variables. Size and QR.pax final positioning were not measured in the same individual but in an isogenic population. To consider the variance in both axes for the regressions, we used a bootstrapping approach with 1000 iterations. Each iteration was made by subsampling 20 egg size measurements, P-to-R distance at hatching, 6 h after hatching and QR.pax final position per genotype. Model 1 regression (Ordinary Least Square method) was performed between each variable at each iteration. Means, intercepts, slopes, R^2_{adj} and *P*-values generated per iteration were saved for plotting. The median of the bootstrapped R^2_{adj} and *P*-values of the regression were used to conclude on the likelihood of the correlation.

Mathematical model for QR.pax final position
For the no-compensation model, we treated the dynamics of the QR cell lineage as one-dimensional, constant-velocity migration within a growing larva. Taking the pharynx to be stationary at the origin $x=0$ and the rectum to be moving away with constant velocity u due to the growth, the length of the pharynx-to-rectum region evolves in time according to

$$l(t) = l_0 + ut, \qquad \text{(Eqn 1)}$$

where l_0 is the length at hatching ($t=0$). The dynamics of the cell position x are:

$$\frac{dx}{dt} = -v(t) + \frac{x}{l(t)}u, \qquad \text{(Eqn 2)}$$

where the first term is the leftward velocity of the cell and the second term is an effective rightward velocity due to the growth. In the second term, we enforce uniform expansion of the larva during growth, such that intermediate points move according to the fraction of the distance to the origin. We assume that the cell begins migrating at a constant velocity v_0 at a

time $t=\tau$ after hatching and stops migrating at a time $t=T$:

$$v(t) = \begin{cases} 0 & t < \tau \\ v_0 & \tau \le t \le T \\ 0 & t > T \end{cases} \qquad \text{(Eqn 3)}$$

Integrating Eqn 2 gives

$$x(t) = \begin{cases} l(t)\dfrac{x_0}{l_0} & t < \tau \\ l(t)\left[\dfrac{x_0}{l_0} - \dfrac{v_0}{u}\ln\left(\dfrac{l(t)}{l(\tau)}\right)\right] & \tau \le t \le T \\ l(t)\left[\dfrac{x_0}{l_0} - \dfrac{v_0}{u}\ln\left(\dfrac{l(T)}{l(\tau)}\right)\right] & t > T \end{cases} \qquad \text{(Eqn 4)}$$

where x_0 is the initial position of the cell. The relative position on the semi-discrete scale is $p=Nx/l$, where $N=27$ (Fig. 1B). Inserting Eqn 4, we have

$$p(t) = \begin{cases} p_0 & t < \tau \\ p_0 - \dfrac{Nv_0}{u}\ln\left(\dfrac{l(t)}{l(\tau)}\right) & \tau \le t \le T \\ p_0 - \dfrac{Nv_0}{u}\ln\left(\dfrac{l(T)}{l(\tau)}\right) & t > T \end{cases} \qquad \text{(5)}$$

where $p_0=19$ is the initial position of the cell (Fig. 1B). We take $u=(35 \text{ µm})/(6 \text{ h})=5.8$ µm/h from the experiments (Fig. S1E), and $\tau=2$ h and $T=8$ h (Sulston and Horvitz, 1977; Ou and Vale, 2009; Ebbing et al., 2019) from the literature, leaving only v_0 as a fit parameter. Fig. 2C (red curve) shows p versus l_0 from Eqn 5 ($t>T$) with best-fit value $v_0=11.6$ µm/h.

For the partial-compensation model, we used Eqn 4 to infer the cell velocity from measurements of x and l at two time points: $t_1=3$ h and $t_2=6$ h. Calling $x(t_1)=x_1$, $x(t_2)=x_2$, $l(t_1)=l_1$ and $l(t_2)=l_2$ for short, and recognizing that both t_1 and t_2 fall between τ and T, we have from Eqn 4,

$$\frac{x_1}{l_1} = \frac{x_0}{l_0} - \frac{v_0}{u}\ln\left(\frac{l_1}{l(\tau)}\right) \quad \text{and} \qquad \text{(Eqn 6)}$$

$$\frac{x_2}{l_2} = \frac{x_0}{l_0} - \frac{v_0}{u}\ln\left(\frac{l_2}{l(\tau)}\right) \qquad \text{(Eqn 7)}$$

at each time point. Subtracting Eqn 7 from Eqn 6 gives

$$\frac{x_1}{l_1} - \frac{x_2}{l_2} = \frac{v_0}{u}\ln\left(\frac{l_2}{l_1}\right). \qquad \text{(Eqn 8)}$$

Because growth is linear in time (Eqn 1), we have $u=(l_2-l_1)/(t_2-t_1)$. Inserting this expression into Eqn 8 and solving for v_0 gives

$$v_0 = \left(\frac{x_1}{l_1} - \frac{x_2}{l_2}\right)\frac{l_2 - l_1}{(t_2 - t_1)\ln(l_2/l_1)}. \qquad \text{(Eqn 9)}$$

Eqn 9 was used to calculate the cell velocities in the *lon-1(e185)* ($x_1=97.9$ µm, $x_2=73.5$ µm, $l_1=160.1$ µm, $l_2=195.4$ µm) and *sma-1(e30)* ($x_1=69.8$ µm, $x_2=46.1$ µm, $l_1=103.2$ µm, $l_2=110.9$ µm) mutants (Fig. 2E), giving $v_0=13.9$ µm/h and $v_0=9.3$ µm/h, respectively. Assuming a linear relationship between velocity and body size,

$$v_0 = ml_2 + b, \qquad \text{(Eqn 10)}$$

the two values of v_0 and l_2 imply $m=0.054$ h^{-1} and $b=3.3$ µm/h. Recognizing that $l_2=l_0+ut_2$, Eqn 10 becomes

$$v_0 = m(l_0 + ut_2) + b, \qquad \text{(Eqn 11)}$$

with $ut_2=35$ µm (Fig. S1E). Fig. 2C (purple curve) shows p versus l_0 from Eqn 5 ($t>T$) with Eqn 11 inserted for v_0.

Control of the maternal age
To test the effect of maternal age, we measured QR.pax final position and P-to-R distance at hatching on progeny from 1-, 2- and 3-day-old hermaphrodite adults (called day 1, day 2 and day 3). L4 larvae were transferred to fresh plates for 27 h to allow them to pass the L4/Adult transition and lay their first embryos (day 1). The same adults were then transferred to a new plate and allowed to lay for 24 h (day 2). Finally, we

repeated this step to obtain the day 3 progeny. The two independent replicates of this experiment were performed at 17°C. The effect of maternal age, genotype and their interaction (if significant) on body size and QR.pax final position was analyzed with a linear mixed model considering the two independent replicates as a random factor. The same data were used to assess QR.pax final position and body size relationships among the four strains. We performed a linear mixed model to explain QR.pax final position by the P-to-R distance at hatching and the genotype as fixed factors, and the two replicates as a random factor. Post-hoc tests to compare different ages were performed with the Tukey contrasts function from the multcomp R package.

Robustness to environmental perturbations

To test the robustness to transient developmental arrest in the L1 stage, we also used two different approaches. In the first approach, the age of the mother was controlled and offspring population were synchronized. We selected embryos using bleach as previously described (Stiernagle, 2006). Briefly, we collected and bleached 1-day-old or 2-day-old hermaphrodites, pelleted embryos and washed the pellet twice with water. We removed the supernatant to retain an embryo pellet of 200 μl, where we added 50 ng of kanamycin and 100 ng of ampicillin. We then plated 100 μl of the egg prep in plate with *E. coli* OP50 and 100 μl in a plate without food. We left the worms without food for around 40 h (Fig. 4A). In the second approach, *C. elegans* cultures were grown until food depletion. Once food was exhausted on the plate, we maintained the population under starvation for 2 more days (Fig. S3A). This protocol avoided a bleach treatment that may affect the larvae independently of the starvation period. We found that, using this protocol, 58% of animals have QR.pa divided above the seam cell V1, 24% with QR.pa at the top of V2, 12% at the top of V3 and 6% at V4 (*n*=50 worms). During this experiment, the positions of BDU, ALM, CAN, HSN and QR.pax were measured in XZ1516 in parallel. The same method was then used in an independent experiment using the genotype N2 (Fig. S3B). After food deprivation in both approaches, we collected starved larvae in M9 buffer and plated them onto NGM agar plates with *E. coli* OP50. We scored QR.pax position 6-8 h later at a precise developmental timepoint: only when V seam cells divided once, Pn cells migrated ventrally, QR.pap reached the dorsal part of the animal and QR.paa the ventral part. We thus did not score the most delayed animals – rejecting these animals is unlikely to be the reason for the observed increased variance in QR.pax position. We performed a Levene's test for equality of variances to measure the effect of the strain and the starvation condition on QR.pax final position variance, adjusted with Bonferroni correction for multiple testing.

In order to test the robustness of QR.pax final position to growth at different temperatures, we transferred day 1 hermaphrodites from 20°C to 15°C, 20°C and 25°C, let them lay for 8 h and removed them from the plate by washing. We then measured QR.pax final position on their offspring. We performed two independent replicates with this method (Fig. 4B). Independently, we used another approach without controlling for the age of the mother. Briefly, L1 larvae from the N2 strain and three wild isolates were transferred from 20°C to 15°C, 20°C or 25°C one generation before scoring. We repeated this experiment three independent times (Fig. S3C). To consider the variability in the response to temperature, we modelled the replicate effect as a random effect. We tested the correlation between QR.pax final position and the absolute value of the latitude of the wild isolate sampling location (as a proxy for the temperature of origin), using Pearson's product-moment correlation test.

Statistical analyses, plots and raw data

Statistical analyses and plots were performed using R version 3.5.2 (R core Team, 2018), R studio version 1.1.463 (Rstudio Team, 2015) and the following packages: car (Fox and Weisberg, 2019), lmerTest (Kuznetsova et al., 2017), effects (Fox and Weisberg, 2018), multcomp (Hothorn et al., 2008), Rmisc (Hope, 2013), ggplot2 (Wickham, 2016), ggstance (Henry et al., 2019) and ggrepel (Slowikowski, 2019). The distribution of QR.pax final position in Figs 1C, 4A, 5A, Figs S1B and S3A,B, was represented with ggridges (Wilke, 2018) using a bandwidth of 0.25 for smoothing. Raw data and summary are presented in the Table S1.

Author contributions

Conceptualization: C.D., S.G., A.M., M.-A.F.; Methodology: C.D., M.-A.F.; Formal analysis: S.G.; Investigation: C.D.; Writing - original draft: C.D., S.G., A.M., M.-A.F.; Visualization: C.D.; Supervision: A.M., M.-A.F.; Funding acquisition: A.M., M.-A.F.

References

Abercrombie, M., Heaysman, J. E. M. and Pegrum, S. M. (1970). The locomotion of fibroblasts in culture: III. Movements of particles on the dorsal surface of the leading lamella. *Exp. Cell Res.* **62**, 389-398. doi:10.1016/0014-4827(70)90570-7

Altun, Z. F. and Hall, D. H. (2020). Handbook of *C. elegans* anatomy. In WormAtlas. http://www.wormatlas.org/hermaphrodite/hermaphroditehomepage.htm

Aman, A. and Piotrowski, T. (2010). Cell migration during morphogenesis. *Dev. Biol.* **341**, 20-33. doi:10.1016/j.ydbio.2009.11.014

Barkai, N. and Leibler, S. (1997). Robustness in simple biochemical networks. *Nature* **387**, 913-917. doi:10.1038/43199

Baugh, L. R. (2013). To grow or not to grow: nutritional control of development during *Caenorhabditis elegans* L1 Arrest. *Genetics* **194**, 539-555. doi:10.1534/genetics.113.150847

Braendle, C. and Félix, M.-A. (2008). Plasticity and errors of a robust developmental system in different environments. *Dev. Cell* **15**, 714-724. doi:10.1016/j.devcel.2008.09.011

Branda, C. S. and Stern, M. J. (2000). Mechanisms controlling sex myoblast migration in *Caenorhabditis elegans* hermaphrodites. *Dev. Biol.* **226**, 137-151. doi:10.1006/dbio.2000.9853

Brenner, S. (1974). The genetics of *Caenorhabditis elegans*. *Genetics* **77**, 71-94. doi:10.1093/genetics/77.1.71

Burke, S. L., Hammell, M. and Ambros, V. (2015). Robust distal tip cell pathfinding in the face of temperature stress is ensured by two conserved microRNAS in *Caenorhabditis elegans*. *Genetics* **200**, 1201-1218. doi:10.1534/genetics.115.179184

Chalfie, M. and Sulston, J. (1981). Developmental genetics of the mechanosensory neurons of *Caenorhabditis elegans*. *Dev. Biol.* **82**, 358-370. doi:10.1016/0012-1606(81)90459-0

Ch'ng, Q., Williams, L., Lie, Y. S., Sym, M., Whangbo, J. and Kenyon, C. (2003). Identification of genes that regulate a Left-Right asymmetric neuronal migration in *Caenorhabditis elegans*. *Genetics* **164**, 1355-1367.

Choy, R. K. M. and Thomas, J. H. (1999). Fluoxetine-resistant mutants in *C. elegans* define a novel family of transmembrane proteins. *Mol. Cell* **4**, 143-152. doi:10.1016/S1097-2765(00)80362-7

Cook, D. E., Zdraljevic, S., Tanny, R. E., Seo, B., Riccardi, D. D., Noble, L. M., Rockman, M. V., Alkema, M. J., Braendle, C., Kammenga, J. E. et al. (2016). The genetic basis of natural variation in *Caenorhabditis elegans* telomere length. *Genetics* **204**, 371-383. doi:10.1534/genetics.116.191148

Cook, D. E., Zdraljevic, S., Roberts, J. P. and Andersen, E. C. (2017). CeNDR, the *Caenorhabditis elegans* natural diversity resource. *Nucleic Acids Res.* **45**, D650-D657. doi:10.1093/nar/gkw893

Coudreuse, D. Y. M., Roël, G., Betist, M. C., Destrée, O. and Korswagen, H. C. (2006). Wnt gradient formation requires retromer function in Wnt-producing cells. *Science* **312**, 921-924. doi:10.1126/science.1124856

Doitsidou, M., Reichman-Fried, M., Stebler, J., Köprunner, M., Dörries, J., Meyer, D., Esguerra, C. V., Leung, T. C. and Raz, E. (2002). Guidance of primordial germ cell migration by the chemokine SDF-1. *Cell* **111**, 647-659. doi:10.1016/S0092-8674(02)01135-2

Duchek, P., Somogyi, K., Jékely, G., Beccari, S. and Rørth, P. (2001). Guidance of cell migration by the *Drosophila* PDGF/VEGF receptor. *Cell* **107**, 17-26. doi:10.1016/S0092-8674(01)00502-5

Ebbing, A., Middelkoop, T. C., Betist, M. C., Bodewes, E. and Korswagen, H. C. (2019). Partially overlapping guidance pathways focus the activity of UNC-40/DCC along the anteroposterior axis of polarizing neuroblasts. *Development* **146**, dev180059. doi:10.1242/dev.180059

Elowitz, M. B., Levine, A. J., Siggia, E. D. and Swain, P. S. (2002). Stochastic gene expression in a single cell. *Science* **297**, 1183-1186. doi:10.1126/science.1070919

Endres, R. G. and Wingreen, N. S. (2008). Accuracy of direct gradient sensing by single cells. *Proc. Natl. Acad. Sci. USA* **105**, 15749-15754. doi:10.1073/pnas.0804688105

Farhadifar, R., Baer, C. F., Valfort, A.-C., Andersen, E. C., Müller-Reichert, T., Delattre, M. and Needleman, D. J. (2015). Scaling, selection, and evolutionary dynamics of the mitotic spindle. *Curr. Biol.* **25**, 732-740. doi:10.1016/j.cub.2014.12.060

Félix, M.-A. and Wagner, A. (2008). Robustness and evolution: concepts, insights and challenges from a developmental model system. *Heredity* **100**, 132-140. doi:10.1038/sj.hdy.6800915

Fleming, T. C., Wolf, F. W. and Garriga, G. (2005). Sensitized genetic backgrounds reveal a role for *C. elegans* FGF EGL-17 as a repellent for migrating CAN neurons. *Development* **132**, 4857-4867. doi:10.1242/dev.02020

Forrester, W. C. and Garriga, G. (1997). Genes necessary for *C. elegans* cell and growth cone migrations. *Development* **124**, 1831-1843.

Fox, J. and Weisberg, S. (2018). Visualizing fit and lack of fit in complex regression models with predictor effect plots and partial residuals. *J. Stat. Softw.* **87**, 1-27. doi:10.18637/jss.v087.i09

Fox, J. and Weisberg, S. (2019). An R Companion to Applied Regression. https://socialsciences.mcmaster.ca/jfox/Books/Companion/

Gallegos, M. E. and Bargmann, C. I. (2004). Mechanosensory neurite termination and tiling depend on SAX-2 and the SAX-1 kinase. *Neuron* **44**, 239-249. doi:10.1016/j.neuron.2004.09.021

Gimond, C., Vielle, A., Silva-Soares, N., Zdraljevic, S., McGrath, P. T., Andersen, E. C. and Braendle, C. (2019). Natural variation and genetic determinants of *Caenorhabditis elegans* sperm size. *Genetics* **213**, 615-632. doi:10.1534/genetics.119.302462

Gómez-Orte, E., Cornes, E., Zheleva, A., Sáenz-Narciso, B., de Toro, M., Iñiguez, M., López, R., San-Juan, J.-F., Ezcurra, B., Sacristán, B. et al. (2017). Effect of the diet type and temperature on the *C. elegans* transcriptome. *Oncotarget* **9**, 9556-9571. doi:10.18632/oncotarget.23563

Grimbert, S., Tietze, K., Barkoulas, M., Sternberg, P. W., Félix, M.-A. and Braendle, C. (2016). Anchor cell signaling and vulval precursor cell positioning establish a reproducible spatial context during *C. elegans* vulval induction. *Dev. Biol.* **416**, 123-135. doi:10.1016/j.ydbio.2016.05.036

Gutteling, E. W., Riksen, J. A. G., Bakker, J. and Kammenga, J. E. (2007). Mapping phenotypic plasticity and genotype–environment interactions affecting life-history traits in *Caenorhabditis elegans*. *Heredity* **98**, 28-37. doi:10.1038/sj.hdy.6800894

Halfter, W., Dong, S., Yip, Y.-P., Willem, M. and Mayer, U. (2002). A critical function of the Pial Basement Membrane in cortical histogenesis. *J. Neurosci.* **22**, 6029-6040. doi:10.1523/JNEUROSCI.22-14-06029.2002

Harris, J., Honigberg, L., Robinson, N. and Kenyon, C. (1996). Neuronal cell migration in *C. elegans*: regulation of Hox gene expression and cell position. *Development* **122**, 3117-3131.

Hedgecock, E. M., Culotti, J. G., Hall, D. H. and Stern, B. D. (1987). Genetics of cell and axon migrations in *Caenorhabditis elegans*. *Development* **100**, 365-382.

Hekimi, S. and Kershaw, D. (1993). Axonal guidance defects in a *Caenorhabditis elegans* mutant reveal cell-extrinsic determinants of neuronal morphology. *J. Neurosci.* **13**, 4254-4271. doi:10.1523/JNEUROSCI.13-10-04254.1993

Hennig, K., Wang, I., Moreau, P., Valon, L., DeBeco, S., Coppey, M., Miroshnikova, Y. A., Albiges-Rizo, C., Favard, C., Voituriez, R. et al. (2020). Stick-slip dynamics of cell adhesion triggers spontaneous symmetry breaking and directional migration of mesenchymal cells on one-dimensional lines. *Sci. Adv.* **6**, eaau5670. doi:10.1126/sciadv.aau5670

Henry, L., Wickham, H. and Chang, W. (2019). ggstance: horizontal "ggplot2" Components. https://CRAN.R-project.org/package=ggstance

Hermann, G. J., Schroeder, L. K., Hieb, C. A., Kershner, A. M., Rabbitts, B. M., Fonarev, P., Grant, B. D. and Priess, J. R. (2005). Genetic analysis of lysosomal trafficking in *Caenorhabditis elegans*. *Mol. Biol. Cell* **16**, 3273-3288. doi:10.1091/mbc.e05-01-0060

Hodgkin, J. and Doniach, T. (1997). Natural variation and copulatory plug formation in *Caenorhabditis elegans*. *Genetics* **146**, 149-164. doi:10.1093/genetics/146.1.149

Hope, R. M. (2013). Rmisc: ryan miscellaneous. https://CRAN.R-project.org/package=Rmisc

Hothorn, T., Bretz, F. and Westfall, P. (2008). Simultaneous inference in General Parametric Models. *Biom. J.* **50**, 346-363. doi:10.1002/bimj.200810425

Inamura, N., Kimura, T., Tada, S., Kurahashi, T., Yanagida, M., Yanagawa, Y., Ikenaka, K. and Murakami, F. (2012). Intrinsic and extrinsic mechanisms control the termination of cortical interneuron migration. *J. Neurosci.* **32**, 6032-6042. doi:10.1523/JNEUROSCI.3446-11.2012

Iwasaki, K., Liu, D. W. and Thomas, J. H. (1995). Genes that control a temperature-compensated ultradian clock in *Caenorhabditis elegans*. *Proc. Natl. Acad. Sci. USA* **92**, 10317-10321. doi:10.1073/pnas.92.22.10317

Johnson, T. E., Mitchell, D. H., Kline, S., Kemal, R. and Foy, J. (1984). Arresting development arrests aging in the nematode *Caenorhabditis elegans*. *Mech. Ageing Dev.* **28**, 23-40. doi:10.1016/0047-6374(84)90150-7

Josephson, M. P., Chai, Y., Ou, G. and Lundquist, E. A. (2016). EGL-20/Wnt and MAB-5/Hox act sequentially to inhibit anterior migration of neuroblasts in *C. elegans*. *PLoS ONE* **11**, e0148658. doi:10.1371/journal.pone.0148658

Kaplan, R. E. W. and Baugh, L. R. (2016). L1 arrest, *daf-16/FoxO* and nonautonomous control of post-embryonic development. *Worm* **5**, e1175196. doi:10.1080/21624054.2016.1175196

Kawano, T., Zheng, H., Merz, D. C., Kohara, Y., Tamai, K. K., Nishiwaki, K. and Culotti, J. G. (2009). *C. elegans mig*-6 encodes papilin isoforms that affect distinct aspects of DTC migration, and interacts genetically with *mig*-17 and collagen IV. *Development* **136**, 1433-1442. doi:10.1242/dev.028472

Kikuchi, T., Shibata, Y., Kim, H.-S., Kubota, Y., Yoshina, S., Mitani, S. and Nishiwaki, K. (2015). The BED finger domain protein MIG-39 halts migration of distal tip cells in *Caenorhabditis elegans*. *Dev. Biol.* **397**, 151-161. doi:10.1016/j.ydbio.2014.10.008

Kim, M., Bjorke, B. and Mastick, G. S. (2019). Motor neuron migration and positioning mechanisms: new roles for guidance cues. *Semin. Cell Dev. Biol.* **85**, 78-83. doi:10.1016/j.semcdb.2017.11.016

Kovacevic, I. and Cram, E. J. (2010). FLN-1/Filamin is required for maintenance of actin and exit of fertilized oocytes from the spermatheca in *C. elegans*. *Dev. Biol.* **347**, 247-257. doi:10.1016/j.ydbio.2010.08.005

Kuznetsova, A., Brockhoff, P. B. and Christensen, R. H. B. (2017). {lmerTest} Package: tests in linear mixed effects models. *J. Stat. Softw.* **82**, 1-26. doi:10.18637/jss.v082.i13

Lau, S., Feitzinger, A., Venkiteswaran, G., Wang, J., Lewellis, S. W., Koplinski, C. A., Peterson, F. C., Volkman, B. F., Meier-Schellersheim, M. and Knaut, H. (2020). A negative-feedback loop maintains optimal chemokine concentrations for directional cell migration. *Nat. Cell Biol.* **22**, 266-273. doi:10.1038/s41556-020-0465-4

Leal-Egaña, A., Letort, G., Martiel, J.-L., Christ, A., Vignaud, T., Roelants, C., Filhol, O. and Théry, M. (2017). The size-speed-force relationship governs migratory cell response to tumorigenic factors. *Mol. Biol. Cell* **28**, 1612-1621. doi:10.1091/mbc.e16-10-0694

Lee, I., Hendrix, A., Kim, J., Yoshimoto, J. and You, Y.-J. (2012). Metabolic rate regulates L1 longevity in *C. elegans*. *PLOS ONE* **7**, e44720. doi:10.1371/journal.pone.0044720

Lee, D., Zdraljevic, S., Cook, D. E., Frézal, L., Hsu, J.-C., Sterken, M. G., Riksen, J. A. G., Wang, J., Kammenga, J. E., Braendle, C. et al. (2019). Selection and gene flow shape niche-associated variation in pheromone response. *Nat. Ecol. Evol.* **3**, 1455-1463. doi:10.1038/s41559-019-0982-3

L'Hernault, S. W., Shakes, D. C. and Ward, S. (1988). Developmental genetics of chromosome I spermatogenesis-defective mutants in the nematode *Caenorhabditis elegans*. *Genetics* **120**, 435-452. doi:10.1093/genetics/120.2.435

Madl, J. E. and Herman, R. K. (1979). Polyploids and sex determination in *Caenorhabditis elegans*. *Genetics* **93**, 393-402.

Marks, M. E., Castro-Rojas, C. M., Teiling, C., Du, L., Kapatral, V., Walunas, T. L. and Crosson, S. (2010). The genetic basis of laboratory adaptation in *Caulobacter crescentus*. *J. Bacteriol.* **192**, 3678-3688. doi:10.1128/JB.00255-10

Martineau, F. S., Sahu, S., Plantier, V., Buhler, E., Schaller, F., Fournier, L., Chazal, G., Kawasaki, H., Represa, A., Watrin, F. et al. (2018). Correct laminar positioning in the neocortex influences proper dendritic and synaptic development. *Cereb. Cortex* **28**, 2976-2990. doi:10.1093/cercor/bhy113

McAdams, H. H. and Arkin, A. (1997). Stochastic mechanisms in gene expression. *Proc. Natl. Acad. Sci. USA* **94**, 814-819. doi:10.1073/pnas.94.3.814

McGrath, P. T., Rockman, M. V., Zimmer, M., Jang, H., Macosko, E. Z., Kruglyak, L. and Bargmann, C. I. (2009). Quantitative mapping of a digenic behavioral trait implicates globin variation in *C. elegans* sensory behaviors. *Neuron* **61**, 692-699. doi:10.1016/j.neuron.2009.02.012

McKeown, C., Praitis, V. and Austin, J. (1998). *sma-1* encodes a betaH-spectrin homolog required for *Caenorhabditis elegans* morphogenesis. *Development* **125**, 2087-2098.

Meighan, C. M. and Schwarzbauer, J. E. (2007). Control of *C. elegans* hermaphrodite gonad size and shape by *vab*-3/Pax6-mediated regulation of integrin receptors. *Genes Dev.* **21**, 1615-1620. doi:10.1101/gad.1534807

Mentink, R. A., Middelkoop, T. C., Rella, L., Ji, N., Tang, C. Y., Betist, M. C., van Oudenaarden, A. and Korswagen, H. C. (2014). Cell intrinsic modulation of Wnt signaling controls neuroblast migration in *C. elegans*. *Dev. Cell* **31**, 188-201. doi:10.1016/j.devcel.2014.08.008

Middelkoop, T. C. and Korswagen, H. C. (2014). Development and migration of the *C. elegans* Q neuroblasts and their descendants. In *WormBook* (ed. The C. elegans Research Community), doi:10.1895/wormbook.1.173.1, http://www.wormbook.org.

Modzelewska, K., Lauritzen, A., Hasenoeder, S., Brown, L., Georgiou, J. and Moghal, N. (2013). Neurons refine the *Caenorhabditis elegans* body plan by directing axial patterning by Wnts. *PLoS Biol.* **11**, e1001465. doi:10.1371/journal.pbio.1001465

Morita, K., Flemming, A. J., Sugihara, Y., Mochii, M., Suzuki, Y., Yoshida, S., Wood, W. B., Kohara, Y., Leroi, A. M. and Ueno, N. (2002). A *Caenorhabditis elegans* TGF-β, DBL-1, controls the expression of LON-1, a PR-related protein, that regulates polyploidization and body length. *EMBO J.* **21**, 1063-1073. doi:10.1093/emboj/21.5.1063

Nigon, V. (1951a). Polyploïdie expérimentale chez un nématode libre, *Rhabditis elegans Maupas*. *Bull. Biol. Fr. Belg.* **85**, 187-225.

Nykamp, K., Lee, M.-H. and Kimble, J. (2008). *C. elegans* La-related protein, LARP-1, localizes to germline P bodies and attenuates Ras-MAPK signaling during oogenesis. *RNA* **14**, 1378-1389. doi:10.1261/rna.1066008

Olmedo, M., Mata-Cabana, A., Rodríguez-Palero, M. J., García-Sánchez, S., Fernández-Yañez, A., Merrow, M. and Artal-Sanz, M. (2020). Prolonged quiescence delays somatic stem cell-like divisions in *Caenorhabditis elegans* and is controlled by insulin signaling. *Aging Cell* **19**, e13085. doi:10.1111/acel.13085

Olsen, A., Vantipalli, M. C. and Lithgow, G. J. (2006). Checkpoint proteins control survival of the postmitotic cells in *Caenorhabditis elegans*. *Science* **312**, 1381-1385. doi:10.1126/science.1124981

Ou, G. and Vale, R. D. (2009). Molecular signatures of cell migration in *C. elegans* Q neuroblasts. *J. Cell Biol.* **185**, 77-85. doi:10.1083/jcb.200812077

Paksa, A., Bandemer, J., Hoeckendorf, B., Razin, N., Tarbashevich, K., Minina, S., Meyen, D., Biundo, A., Leidel, S. A., Peyrieras, N. et al. (2016). Repulsive cues combined with physical barriers and cell–cell adhesion determine progenitor cell positioning during organogenesis. *Nat. Commun.* **7**, 1-14. doi:10.1038/ncomms11288

Pani, A. M. and Goldstein, B. (2018). Direct visualization of a native Wnt in vivo reveals that a long-range Wnt gradient forms by extracellular dispersal. *eLife* **7**, e38325. doi:10.7554/eLife.38325

Perez, M. F., Francesconi, M., Hidalgo-Carcedo, C. and Lehner, B. (2017). Maternal age generates phenotypic variation in *Caenorhabditis elegans*. *Nature* **552**, 106-109. doi:10.1038/nature25012

Qu, Z., Ji, S. and Zheng, S. (2020). Glucose and cholesterol induce abnormal cell divisions via DAF-12 and MPK-1 in *C. elegans*. *Aging (Albany NY)* **12**, 16255-16269. doi:10.18632/aging.103647

R core Team (2018). R: a language and environment for statistical computing. https://www.R-project.org/.

Rabbitts, B. M., Ciotti, M. K., Miller, N. E., Kramer, M., Lawrenson, A. L., Levitte, S., Kremer, S., Kwan, E., Weis, A. M. and Hermann, G. J. (2008). *glo-3*, a Novel *Caenorhabditis elegans* gene, is required for lysosome-related organelle biogenesis. *Genetics* **180**, 857-871. doi:10.1534/genetics.108.093534

Rella, L., Fernandes Póvoa, E. E. and Korswagen, H. C. (2016). The *Caenorhabditis elegans* Q neuroblasts: a powerful system to study cell migration at single-cell resolution *in vivo*. *Genesis* **54**, 198-211. doi:10.1002/dvg.22931

Ridley, A. J., Schwartz, M. A., Burridge, K., Firtel, R. A., Ginsberg, M. H., Borisy, G., Parsons, J. T. and Horwitz, A. R. (2003). Cell migration: Integrating signals from front to back. *Science* **302**, 1704-1709. doi:10.1126/science.1092053

Rohrschneider, M. R. and Nance, J. (2013). The union of somatic gonad precursors and primordial germ cells during *C. elegans* embryogenesis. *Dev. Biol.* **379**, 139-151. doi:10.1016/j.ydbio.2013.03.019

RStudio Team. (2015). RStudio: integrated development environment for R. http://www.rstudio.com/.

Sato, M., Sato, K., Liou, W., Pant, S., Harada, A. and Grant, B. D. (2008). Regulation of endocytic recycling by *C. elegans* Rab35 and its regulator RME-4, a coated-pit protein. *EMBO J.* **27**, 1183-1196. doi:10.1038/emboj.2008.54

Silhankova, M. and Korswagen, H. C. (2007). Migration of neuronal cells along the anterior-posterior body axis of *C. elegans*: Wnts are in control. *Curr. Opin. Genet. Dev.* **17**, 320-325. doi:10.1016/j.gde.2007.05.007

Slowikowski, K. (2019). ggrepel: Automatically position non-overlapping text labels with "ggplot2". https://CRAN.R-project.org/package=ggrepel.

Spudich, J. L. and Koshland, D. E. (1976). Non-genetic individuality: chance in the single cell. *Nature* **262**, 467-471. doi:10.1038/262467a0

Stanley, C. E. and Kulathinal, R. J. (2016). Genomic signatures of domestication on neurogenetic genes in *Drosophila melanogaster*. *BMC Evol. Biol.* **16**, 6. doi:10.1186/s12862-015-0580-1

Sterken, M. G., Snoek, L. B., Kammenga, J. E. and Andersen, E. C. (2015). The laboratory domestication of *Caenorhabditis elegans*. *Trends Genet.* **31**, 224-231. doi:10.1016/j.tig.2015.02.009

Stiernagle, T. (2006). Maintenance of *C. elegans*. In WormBook (ed. The *C. elegans* Research Community), doi:10.1895/wormbook.1.101.1, http://www.wormbook.org.

Sulston, J. E. and Horvitz, H. R. (1977). Post-embryonic cell lineages of the nematode, *Caenorhabditis elegans*. *Dev. Biol.* **56**, 110-156. doi:10.1016/0012-1606(77)90158-0

Sulston, J. E., Schierenberg, E., White, J. G. and Thomson, J. N. (1983). The embryonic cell lineage of the nematode *Caenorhabditis elegans*. *Dev. Biol.* **100**, 64-119. doi:10.1016/0012-1606(83)90201-4

Svitkina, T. (2018). The actin cytoskeleton and actin-based motility. *Cold Spring Harb. Perspect. Biol.* **10**, a018267. doi:10.1101/cshperspect.a018267

Szabó, A. and Mayor, R. (2018). Mechanisms of neural crest migration. *Annu. Rev. Genet.* **52**, 43-63. doi:10.1146/annurev-genet-120417-031559

The C. elegans Deletion Mutant Consortium. (2012). Large-scale screening for targeted knockouts in the *Caenorhabditis elegans* genome. *G3 Genes Genomes Genet.* **2**, 1415-1425. doi:10.1534/g3.112.003830

van Helvert, S., Storm, C. and Friedl, P. (2018). Mechanoreciprocity in cell migration. *Nat. Cell Biol.* **20**, 8-20. doi:10.1038/s41556-017-0012-0

Whangbo, J. and Kenyon, C. (1999). A Wnt signaling system that specifies two patterns of cell migration in *C. elegans*. *Mol. Cell* **4**, 851-858. doi:10.1016/S1097-2765(00)80394-9

White, J. G., Southgate, E., Thomson, J. N. and Brenner, S. (1986). The structure of the nervous system of the nematode *Caenorhabditis elegans*. *Phil. Trans. R. Soc. Lond. B* **314**, 1-340. doi:10.1098/rstb.1986.0056

Wickham, H. (2016). *ggplot2: Elegant Graphics for Data Analysis*. New York: Springer-Verlag.

Wilke, C. O. (2018). ggridges: Ridgeline Plots in "ggplot2". https://CRAN.R-project.org/package=ggridges.

Yamamoto, K. and Kimura, A. (2017). An asymmetric attraction model for the diversity and robustness of cell arrangement in nematodes. *Development* **144**, 4437-4449. doi:10.1242/dev.154609

Zheng, S., Chiu, H., Boudreau, J., Papanicolaou, T., Bendena, W. and Chin-Sang, I. (2018). A functional study of all 40 *Caenorhabditis elegans* insulin-like peptides. *J. Biol. Chem.* **293**, 16912-16922. doi:10.1074/jbc.RA118.004542

Zhu, Z., Chai, Y., Jiang, Y., Li, W., Hu, H., Li, W., Wu, J.-W., Wang, Z.-X., Huang, S. and Ou, G. (2016). Functional coordination of WAVE and WASP in *C. elegans* neuroblast migration. *Dev. Cell* **39**, 224-238. doi:10.1016/j.devcel.2016.09.029

Zinovyeva, A. Y. and Forrester, W. C. (2005). The *C. elegans* Frizzled CFZ-2 is required for cell migration and interacts with multiple Wnt signaling pathways. *Dev. Biol.* **285**, 447-461. doi:10.1016/j.ydbio.2005.07.014

Zinovyeva, A. Y., Yamamoto, Y., Sawa, H. and Forrester, W. C. (2008). Complex network of wnt signaling regulates neuronal migrations during *Caenorhabditis elegans* development. *Genetics* **179**, 1357-1371. doi:10.1534/genetics.108.090290